Electrochimica Acta 54 (2009) 4963–4970

Contents lists available at ScienceDirect

Electrochimica Acta

journal homepage: www.elsevier.com/locate/electacta

Computer simulation and SERR detection of cytochrome *c* dynamics at SAM-coated electrodes

Damián Alvarez Paggi[a], Diego F. Martín[a], Anja Kranich[b], Peter Hildebrandt[b], Marcelo A. Martí[a,*], Daniel H. Murgida[a,*,1]

[a] *Departamento de Química Inorgánica, Analítica y Química Física/INQUIMAE-CONICET, Facultad de Ciencias Exactas y Naturales, Universidad de Buenos Aires, Ciudad Universitaria, Pab. 2, piso 1, C1428EHA Buenos Aires, Argentina*
[b] *Institut für Chemie, Technische Universität Berlin, Str. des 17, Juni 135, Sekr. PC14, D-10623 Berlin, Germany*

ARTICLE INFO

Article history:
Received 28 November 2008
Received in revised form 13 February 2009
Accepted 13 February 2009
Available online 26 February 2009

Keywords:
Protein electron transfer
SERR
Cytochrome *c*
Molecular dynamics
Self-assembled monolayers

ABSTRACT

In this paper we present a combined experimental and theoretical study of the heterogeneous electron transfer reaction of cytochrome *c* electrostatically adsorbed on metal electrodes coated with monolayers of 6-mercaptohexanoic acid. Molecular dynamics simulations and pathways calculations show that adsorption of the protein leads to a broad distribution of orientations and, thus, to a correspondingly broad distribution of electron transfer rate constants due to the orientation-dependence of the electronic coupling parameter. The adsorbed protein exhibits significant mobility and, therefore, the measured reaction rate is predicted to be a convolution of protein dynamics and tunnelling probabilities for each orientation. This prediction is confirmed by time-resolved surface enhanced resonance Raman which allows for the direct monitoring of protein (re-)orientation and electron transfer of the immobilised cytochrome *c*. The results provide a consistent explanation for the non-exponential distance-independence of electron transfer rates usually observed for proteins immobilized on electrodes.

© 2009 Elsevier Ltd. All rights reserved.

1. Introduction

Direct electrochemistry of redox proteins immobilized on electrodes represents an active field of research for a number of reasons. First, electrochemical experiments with adsorbed species require significantly lower amounts of sample and interpretation of the results is largely simplified compared to solution electrochemistry. Thus, determination of thermodynamic and kinetic parameters, as well as elucidation of mechanistic aspects of redox enzymes is readily possible [1–3]. Second, there is a growing interest in the development of devices such as sensors and biofuel cells based on immobilized redox enzymes [4–6].

A widely used strategy for immobilizing proteins under preservation of the native structure is based on coating the electrode surface with self-assembled monolayers (SAMs) of ω-functionalized alkanethiols. The tail groups of the thiols are selected according to the surface properties of the protein in order to achieve efficient immobilization through electrostatic or hydrophobic interactions as well as via cross linking and coordinative bonds [7,8].

A specific advantage of these immobilization techniques is that they allow for the investigation of the distance dependence of the electron transfer (ET) rates by simply changing the lengths of the alkanethiols without modifying other parameters. Studies of this kind have been reported for a number of proteins which are quite diverse in terms of structure, redox active center, surface properties and, therefore, modes of immobilization [7,9–15]. In spite of the differences, the distance dependence of the measured ET rate constants (k_{ET}^{app}) is qualitatively similar in all these cases. At long distances (i.e. SAMs containing more than 10 CH_2-groups) k_{ET}^{app} follows the expected exponential dependence predicted by the theory for nonadiabatic electrochemical reactions. For thinner SAMs, however, k_{ET}^{app} becomes distance independent. The origin for this behaviour has been elusive and controversial.

This is also true for cytochrome *c* (Cyt), a soluble heme protein that acts as an electron carrier in the mitochondrial respiratory chain and represents an ideal model system for electrochemical and spectroelectrochemical studies. The distance dependence of k_{ET}^{app} for Cyt has been investigated using different experimental techniques and immobilization procedures. These include electrostatic adsorption to electrodes coated with SAMs of ω-carboxylalkanethiols [9,11,16,17] and direct wiring of the redox center via pyridinil-terminated SAMs that coordinate the heme-iron by displacing the Met natural axial ligand [13,18–21]. In both cases, the variation of the rate constant with decreasing distance is qualitatively similar,

* Corresponding authors. Tel.: +54 11 4576 3378x124; fax: +54 11 4576 3341.
E-mail addresses: marcelo@qi.fcen.uba.ar (M.A. Martí), dhmurgida@qi.fcen.uba.ar (D.H. Murgida).
[1] ISE member.

0013-4686/$ – see front matter © 2009 Elsevier Ltd. All rights reserved.
doi:10.1016/j.electacta.2009.02.050

i.e., the rate increases exponentially for long tethers but levels off to constant value for shorter ones. Three models have been proposed for rationalizing these results: (i) a change of the ET regime from nonadiabatic at long distances to friction controlled at short ones [20,21]; (ii) a two states model in which Cyt is assumed to bind in an electrochemically inactive configuration and needs to reorient to the active state, with reorientation being rate limiting at short distances [11] and (iii) an electric field controlled reaction [9,22]. All these models have been originally proposed based on sound but indirect evidence that does not allow for an unambiguous distinction between the three mechanisms.

Recently, we have reported a two-colour time resolved surface enhanced resonance Raman (TR-SERR) study in which we provide the first direct evidence that the rate limiting step for the reduction of Cyt electrostatically adsorbed on SAMs of short ω-carboxylalkanethiols is indeed protein reorientation, and that this process is most likely controlled by the interfacial electric field [23].

Here we have extended these studies and complemented them with molecular dynamics (MD) simulations. The combination of TR-SERR experiments and computer simulations provides an unprecedented detailed picture of the electrochemical reaction of Cyt at interfaces and opens new perspectives for studying bioelectrochemical processes in general.

2. Experimental

2.1. Chemicals

6-Mercaptohexanoic acid (C_5) was purchased from Dojindo and used without further purification. Horse heart cytochrome *c* (Cyt) was purchased from Sigma–Aldrich and purified by HPLC. All other chemicals were of the higher available purity. Solutions were prepared with deionized water ($R \geq 18\,M\Omega$; Millipore).

2.2. SERR measurements

After mechanical polishing silver ring electrodes were subjected to oxidation–reduction cycles in KCl 0.1 M to create a SER-active nanostructured surface and, subsequently, were incubated in 1 mM ethanolic solutions of C_5 for 24 h, rinsed and transferred to the spectroelectrochemical cell. In addition to the rotating Ag ring working electrode, the SERR spectroelectrochemical cell contains a Pt wire and a Ag/AgCl electrode as counter and reference electrodes, respectively. All potentials cited in this work refer to the Ag/AgCl (3 M KCl) electrode. During SERR measurements the working electrode was rotated at ca. 5 Hz to avoid laser-induced sample degradation. The electrolyte solution (12.5 mM phosphate buffer, pH 7.0; 12.5 mM K_2SO_4) was bubbled with Ar prior to the measurements and Ar overpressure was maintained along experiments. Protein adsorption was achieved by 15 min incubation of the SAM coated electrode in the SERR cell containing 0.2 μM Cyt in the working electrolyte.

SERR spectra were measured in back-scattering geometry using a confocal microscope coupled to a single stage spectrograph (Jobin Yvon, LabRam 800 HR) equipped with a 2400 l/mm grating and liquid nitrogen cooled back illuminated CCD detector. Elastic scattering was rejected with Notch filters. The 413 nm line of a cw Krypton ion laser (Coherent Innova 300c) or the 514 nm line of a cw Argon laser (Coherent Innova 70c) were focused onto the surface of the Ag rotating electrode by means of a long working distance objective (20×; N.A. 0.35).

Typically, experiments were performed with laser powers of ca. 1 mW (413 nm) and 12 mW (514 nm) at sample. Effective acquisition times were 2–6 s. Increments per data point of 0.57 cm^{-1} and spectral resolutions of 2 cm^{-1} were used at 413 nm excitation. All experiments were repeated several times to ensure reproducibility.

For TR-SERR experiments, potential jumps of variable height and duration were applied for triggering the reaction. SERR spectra were measured at variable delay times after each jump. Synchronization of potential jumps and probe laser pulses was achieved with a home made four-channel pulse-delay generator. The probe pulses were generated by passing the cw laser beam trough two consecutive laser intensity modulators (Linos). At the end of each jump the electrode potential is set back to the initial value and the system is allowed to relax for a sufficiently long time in order to fully recover the fresh sample condition. The entire sequence is repeated until reaching effective acquisition times of ca. 2–6 s which provide acceptable signal-to-noise ratios.

After background subtraction the spectra were treated by band fitting (514 nm) or by component analysis (413 nm) in which the spectra of the individual species were fitted to the experimental spectra using home-made analysis software.

2.3. Computational methods

2.3.1. Set up of the system

Initial Cyt structures were obtained from the PDB database (PDB 1HRC for the reduced form, Cyt^{2+}; and PDB 1OCD for the oxidized form, Cyt^{3+}). To simulate the SAMs an array of 13 × 13 fixed Au atoms with lattice structure 1 1 1 was built *in silico*, and each of them was linked to a C_5 molecule through the S atom. SAM and lattice parameters were adopted from the literature [24]. Au was chosen instead of Ag because the SAM parameters are better defined in the first case. Note that the properties of the nanostructured bulk metal are not reproduced by the calculations and, thus, calculations only have qualitative and comparative value. Consequently, small differences that may exist at the level of the SAMs on the two metals have no consequences for the conclusions drawn. The ionization degree of the carboxyl-terminated SAMs was set to 10%, 25% and 50% in different simulations for comparative studies. All MD simulations were performed using the AMBER package [25], with the ff99 force field implementation. The heme parameters were taken from previous work [26].

2.3.2. Binding of Cyt to the SAMs

Adsorption of Cyt^{2+} and Cyt^{3+} to C_5-SAMs was investigated using steered MD (SMD) [27] starting from equilibrated structures of both protein and SAM. For that purpose, 26 different configurations were generated with Cyt located at ca. 5–10 Å from the SAM surface. The 26 configurations differ in the rotational orientation of the protein with respect to the monolayer and were built by performing rigid body rotations of the Cyt equilibrated structure. Starting from each configuration SMD simulations were performed by pulling the Cyt towards the monolayer at constant velocity, while computing the applied force. The pulling reaction coordinate (RC) is the distance between the central Au atom (which is fixed at the bottom of the SAM) and the center of mass of the Cα atoms of the protein. Integration of the force applied to move the protein towards the monolayer yields the work performed along the RC. In the SMD runs, the generalized Born model [28] was employed for implicit solvation. Using explicit water molecules is computationally too expensive since the resultant solvent viscosity causes very low pulling speeds. The plots of the computed work *vs*. the RC can be taken as an estimate for the free energy profile of the adsorption process.

2.3.3. Explicit water simulations and periodic boundary conditions

Starting from selected structures for the Cyt/SAM complex obtained by SMD simulations, we performed MD simulations in explicit solvent. Here, each SAM/Cyt complex was immersed into a

TIP3P water box, and periodic boundary conditions were applied. In each case an initial constant volume MD was performed to heat system to 300 K and, secondly, a constant pressure run was carried out to equilibrate the system density. Finally, 5 ns productions MD were performed. Temperature and pressure were kept constant using the Berendsen thermostat and barostat [29]. For the PBC simulations Ewald summations are employed to compute the electrostatic energy terms using the default parameters in the sander module of the AMBER package.

2.3.4. Characterization of the Cyt orientation

The orientation of the heme group with respect to the Au/SAM surface is defined in terms of two angles. The first one, α, is the angle between the Fe–S (Met80) bond, which is perpendicular to the heme plane, and the Z-axis. Values of α close to 0° or 180° imply that the heme lies parallel to the SAM, whereas values close to 90° mean that the heme is oriented perpendicular to the surface. The second one, φ, is the angle between the vector defined by the Fe–N (pyrrole A) bond and the vector pointing towards the SAM which is contained by the heme plane. This angle describes the rotational orientation of the heme and is measured counterclockwise with the Fe–S (Met80) vector pointing towards the reader. Values between 270° and 360° correspond to protein orientations where the propionate groups of the heme are closer to the SAM surface, whereas for values between 90° and 180° the propionate groups are pointing away from the SAM surface. It should be noted that for α values close to 0° or to 180° changes of the φ value do not correspond to significant variations of protein orientation since the heme lies parallel to the monolayer surface. Therefore, for the sake of a more intuitive representation that takes into account this effect, the φ axes in plots (α, φ) shown below (Figs. 4 and 6) are transformed according to Eq. (1):

$$\varphi^* = (\varphi - 180)\sqrt{1 - \left(\frac{\alpha - 90}{90}\right)^2} + 180 \quad (1)$$

The actual φ values in these figures are indicated as isolines.

The Cyt/SAM complexes are also characterized by the contact Lys residues. A contact is defined whenever a Lys residue is less than 5 Å apart of a tail group of the SAM.

The protein dipole moment is computed with respect to the center of charge of the protein, as reported by Margoliash [30]; and its orientation is defined as the angle between the dipole vector and the Z-axis which is normal to the SAM plane.

2.3.5. Coupling matrix calculation

Electronic couplings between the heme-iron and any of the gold atoms that represent the electrode surface were estimated using the pathway algorithm developed by Beratan et al. [31,32]. To obtain a proper description of the system, adjustment of the algorithm parameters was required. First, all orbitals of the heme-iron were considered to be equivalent. Second, couplings between atoms of the porphyrin ring was set to 1 in order to reproduce the resonant character. Finally, the coupling between each gold atom was set to 1, such that the electron pathway computations are independent of the gold atom of choice.

3. Results and discussion

3.1. TR-SERR experiments

The dynamics of heterogeneous ET of Cyt adsorbed on nanostructured Ag electrodes coated with C_5-SAMs was investigated by TR-SERR. It has been shown in previous work [23] that SERR spectra of Cyt measured under resonance conditions either with the Soret or Q electronic absorption bands of the heme are dominated by in-plane heme vibrations. The bands in the high frequency region (ca. 1300–1700 cm^{-1}) are sensitive to the redox state, spin and coordination pattern of the heme-iron and, thus, can be used for monitoring the structural integrity of the protein active site as well as the redox reaction. As previously reported, SERR spectra of Cyt^{3+} and Cyt^{2+} under the present immobilization conditions and measured with Soret-band excitation are identical to the corresponding resonance Raman spectra in solution [3,23]. Therefore, we can safely conclude that the protein native structure is preserved upon immobilization on a C_5-coated electrode. This conclusion holds for the three pH values investigated in this work (6.0, 7.0 and 7.8).

The electrochemical reduction of immobilized Cyt following a potential jump was monitored by TR-SERR using Q-band excitation. Compared to Soret-band excitation, this approach has the specific advantage that it allows for monitoring changes in the average protein orientation, in addition to structural and redox state changes. The disadvantage is that signals are significantly weaker compared to Soret-band excitation due to the weaker oscillator strength of the Q-band.

According to SER selection rules it can be shown that the A_{1g} vibrational modes of the porphyrin ring (assumed to be of D_{4h} symmetry) are preferentially enhanced when the protein is oriented with the heme plane perpendicular to the electrode surface. In the other extreme case, i.e. when the heme plane is parallel to the electrode surface, totally symmetric (A_{1g}) and non-totally symmetric modes (A_{2g}, B_{1g} and B_{2g}) are enhanced to a similar extent [23]. Thus, although it is not possible to extract absolute orientations in a reliable manner, changes of the average protein orientation can be tracked by determining the intensity ratio for bands of different symmetry, e.g. B_{1g}/A_{1g}, as a function of time. This principle has been successfully applied for evaluating the orientation of molecules adsorbed on SER-active substrates, including Cyt on Ag colloids [33] and on roughened electrodes [23]. This type of analysis is not possible using Soret-band excitation partially due to the break-down of the SER selection rules under rigorous resonance conditions and the relatively weak contributions of modes other than A_{1g}.

Fig. 1 shows TR-SERR spectra of Cyt on a C_5-SAM measured at different delay times following a reductive potential jump (E° = 25 mV [34]) from 50 to −50 mV at neutral pH and using 514 nm excitation. Note that the overall appearance of the spectra changes with time. We will focus the analysis on the modes ν_4 and ν_{10} that possess A_{1g} and B_{1g} symmetry, respectively.

The ν_4 envelope is composed by a stronger signal at ca. 1360 cm^{-1} and a shoulder at ca. 1372 cm^{-1} which correspond to Cyt^{2+} and Cyt^{3+}, respectively. The respective intensities can be accurately determined by band fitting analysis. The ν_{10} bands of Cyt^{2+} and Cyt^{3+}, on the other hand, are even better resolved and appear at 1621 and 1636 cm^{-1}, respectively. Thus, while redox changes are monitored trough band shifts larger than 10 cm^{-1}, orientation information is obtained from the relative intensities of two bands for the same redox state making the separation of the two possible processes straightforward and unambiguous. Upon applying a potential jump to more negative potentials, the intensities of the ν_4 and ν_{10} bands of Cyt^{3+} decrease in favour of the corresponding bands of Cyt^{2+}. The decay is exponential, as expected for a single step relaxation process. From the time constants one can obtain the apparent ET rate constants (k_{app}^{ET}). However, temporal spectral changes are not restricted to the absolute intensities of the Cyt^{3+} *vs.* Cyt^{2+} bands. A careful band fitting analysis shows that the intensity ratio ν_{10}/ν_4 for Cyt^{3+} also evolves exponentially with time subsequent to the potential jump (Fig. 2A). For comparison, the ν_{10}/ν_4 ratios for the protein in solution are 3.59 and 0.27 for Cyt^{3+} and Cyt^{2+}, respectively. These time-dependent changes are interpreted in terms of reorientation of the adsorbed protein from the average equilibrium orientation at the initial potential to the corresponding values at the final potential. The apparent rate constants of reori-

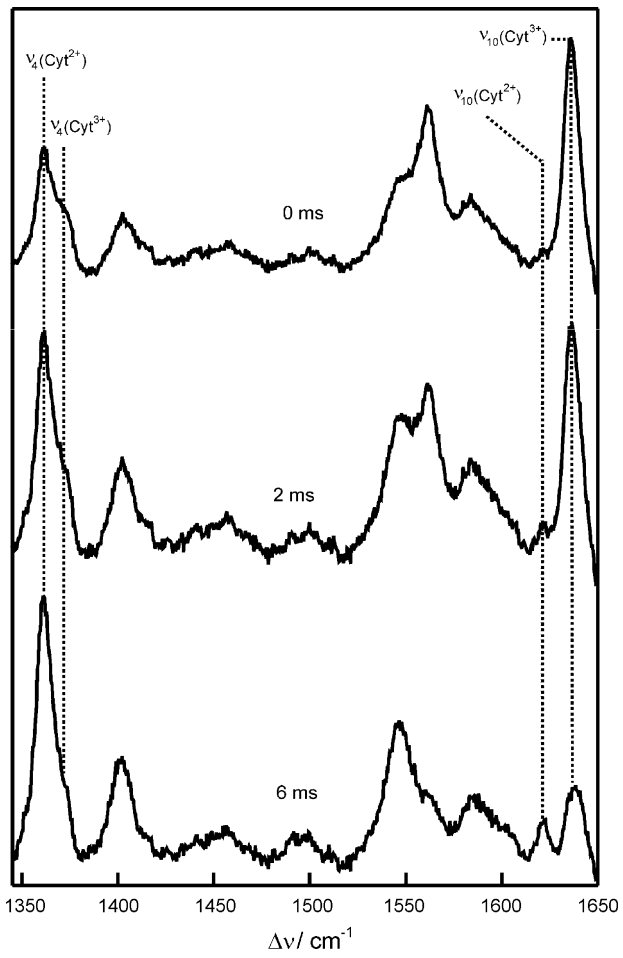

Fig. 1. SERR spectra of Cyt adsorbed to a C_5-SAM measured with 514 nm excitation at variable delay times after applying a potential jump from 50 to −50 mV (pH 7.0).

entation (k_{app}^{reor}) obtained in this way for different pH values are summarized in Fig. 2B and compared with the k_{app}^{ET} values obtained with 413 nm excitation under otherwise identical conditions.

Reorientation and ET rate constants are very similar within experimental error and both decay with increasing pH. The isoelectric point of Cyt is ca. 10 while the pK_a of the C_5-SAM is ca. 8 [34]. Thus, within the pH range employed here, the protonation equilibrium of the SAM is expected to be significantly more affected than that of the protein. Accordingly, one can readily rationalise the decrease of the protein reorientation rate in the electrostatic complex upon increasing the charge density of the SAM, i.e. at higher pH values. Moreover, the observation that the rates of reduction are almost identical to the reorientation rates at every pH suggests that the rate limiting event is not electron tunnelling but protein reorientation. In order to test this hypothesis we performed the simulations described in the following sections.

3.2. Characterization of binding domains

The adsorption of Cyt on a gold surface coated with a C_5-SAM was investigated using SMD. In these simulations the protein is pulled towards the SAM surface at constant velocity starting from a distance of about 5–10 Å, while computing the force applied. Since the pulling force is small and the solvent is only treated implicitly at this stage, the work along the reaction coordinate can be taken as a comparative estimate of the free energy profile for the binding process. In order to map the protein surface for possible binding sites, simulations were performed starting from 26 different rotational orientations with respect to the SAM surface, both for Cyt^{2+} and Cyt^{3+}.

Fig. 3 shows typical work profiles obtained for a non-binding and a binding orientation. While in the first case the applied work increases steadily upon approaching of Cyt to the SAM surface, in the second case a minimum is achieved at contact distance whose deepness gives an estimate of the binding energy.

From the 26 tested orientations only 9 yield stable complexes for Cyt^{2+} and 14 for Cyt^{3+} as evidenced by the presence of minima in the work profiles. The estimated binding energies are summarized in Table 1, as well as the key lysine residues involved in the electrostatic complex for each orientation, and the values for the two characteristic angles which define the orientation of the heme prosthetic group with respect to the Au plane (see above for definition of α and φ). Using these two angles it is possible to construct a map of binding orientations and energies of Cyt on the SAM, as shown in Fig. 4.

Note that although only the upper semicircle of the (α, φ) plot is significantly populated, i.e. $\varphi > 160^\circ$, the distribution of binding orientations is rather broad with $\Delta\alpha \sim 120^\circ$ and $\Delta\varphi \sim 180^\circ$. Taking into account the key lysine residues involved in each electrostatic complex, the different orientations can be clustered into three binding domains: (i) a low affinity domain defined by lysines 22, 39 and 60 (BD1) that is only observed for Cyt^{3+} and has an average binding energy of 0.68 Kcal mol^{-1}; (ii) a medium affinity domain (BD2) with lysines 25 and 27 as key residues and an average binding energy of 0.93 Kcal mol^{-1} (1.18 and 0.67 Kcal mol^{-1} for Cyt^{2+} and

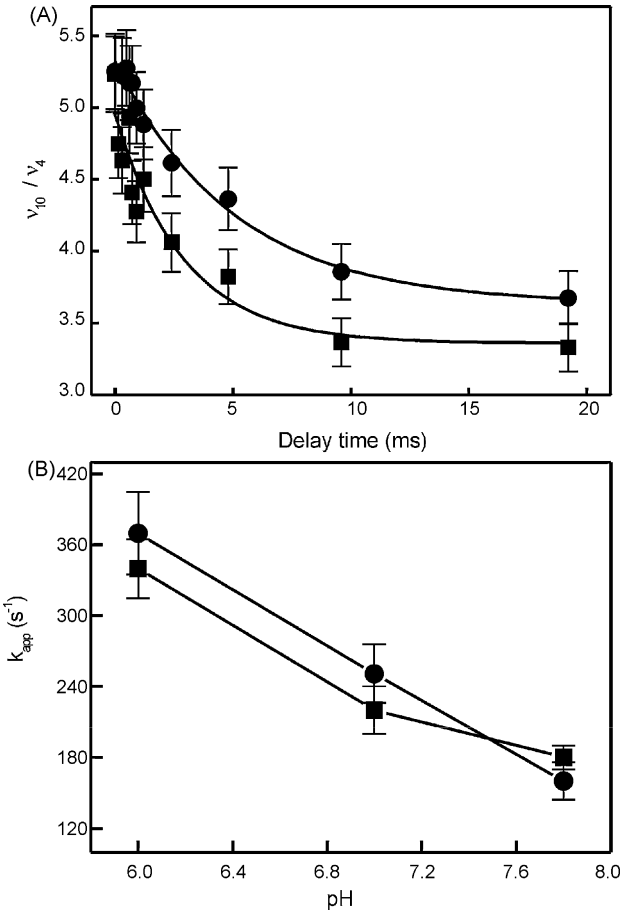

Fig. 2. (A) Time-dependence of the ν_{10}/ν_4 intensity ratio of Cyt^{3+} measured by TR-SERR with 514 nm excitation following a potential from 50 to −50 mV. Circles: pH 7.8. Squares: pH 6.0. (B) Apparent rate constants determined by TR-SERR as a function of the pH. Circles: k_{app}^{reor} measured with 514 nm excitation. Squares: k_{app}^{ET} measured with 413 nm excitation.

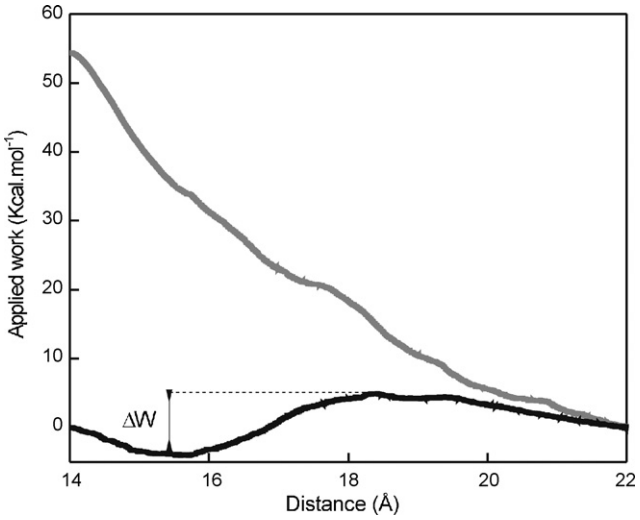

Fig. 3. Work profiles obtained by SMD for the binding of Cyt^{2+} to a C_5-SAM (10% ionization) starting from two different orientations. Grey line: non-binding orientation. Black line: binding orientation. The distance is defined from the center of mass of Cyt to the SAM's surface.

Cyt^{3+}, respectively) and (iii) a high affinity domain (BD3) defined by lysines 72, 73, 79, 86 and 87 with an average binding energy of 2.21 Kcal mol^{-1} (3.34 and 1.09 Kcal mol^{-1} for Cyt^{2+} and Cyt^{3+}, respectively). The location of the different domains on the Cyt surface is represented in Fig. 5.

In contrast to BD1, the binding domains of higher affinity (BD2 and BD3) correspond to orientations in which the solvent exposed part of the heme group points towards the SAM with the heme plane tilted to either side with respect to the Au surface and, therefore, are expected to be relevant for electron transfer.

3.3. Dynamics of the adsorbed protein

In order to study the dynamics of the Cyt/SAM complexes, MD simulations were performed in an explicit water environment for

Table 1
Structural parameters of the Cyt/C_5-SAM stable complexes for a 10% ionized SAM as obtained by SMD[a].

	α	φ	Binding (Kcal mol^{-1})	Key Lysines
	139	217	1.72	72, 73, 79, 86
	124	241	1.91	55, 72, 73, 79
	54	220	1	25, 27
	61	196	1.3	22, 25, 27
Cyt^{2+}	144	324	3.2	55, 73, 87, 88
	153	216	0.7	72, 73, 86
	141	215	10	72, 73, 79, 86, 87
	124	198	2.5	13, 72, 73, 79, 86, 87
	70	172	1.25	8, 25, 27
	124	168	1.68	13, 72, 79, 86, 87
	154	233	0.72	55, 72, 73, 86
	80	208	1.22	25, 27, 79
	84	216	0.262	25, 27, 79
	87	205	0.54	27, 79
	105	342	0.65	39, 53, 55, 60
	157	69	1.07	73, 87, 88
Cyt^{3+}	147	302	1.45	55, 72, 73
	48	324	1	22, 39, 53
	98	349	0.56	39, 60
	41	332	0.2	22
	121	236	0.84	72, 79
	83	356	1	39, 55, 60, 99
	110	240	0.8	72, 79

[a] See Section 2.3 for the definition of angles α and φ.

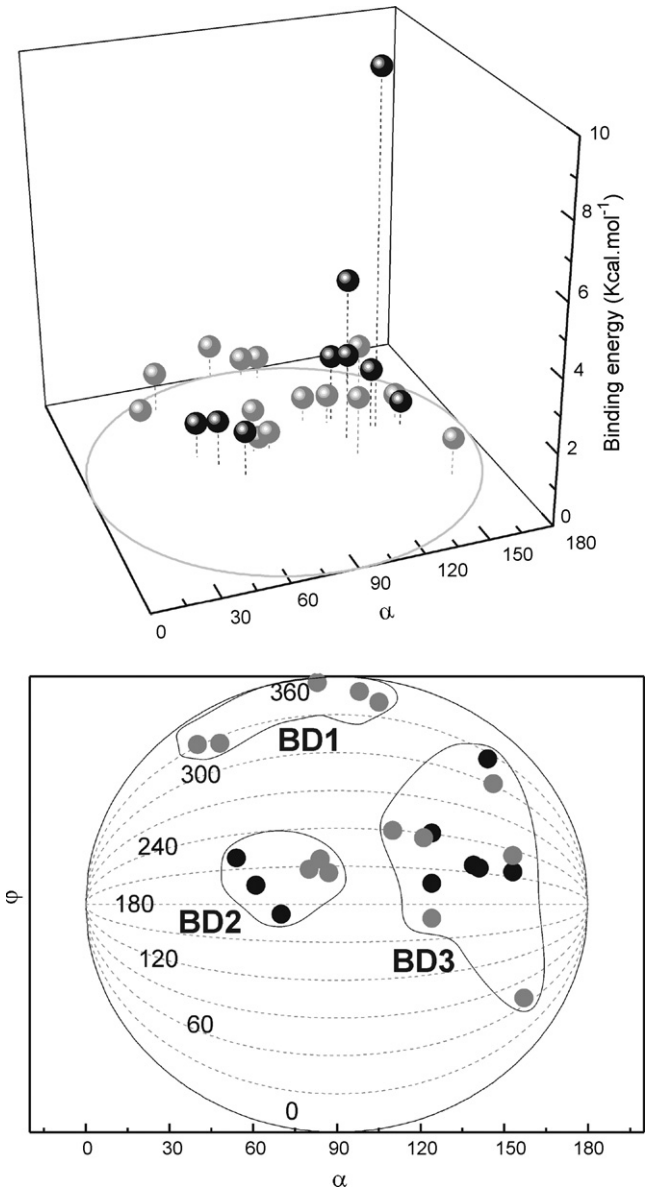

Fig. 4. Top: 3D representation of the orientation parameters and binding energies of Cyt on a C_5-SAM with 10% ionization. Bottom: Projection of A on the (α, φ) plane. Encircled areas represent the different binding domains. Black circles: Cyt^{2+}. Grey circles: Cyt^{3+}. Isolines indicate the φ values.

5 ns, using each of the binding orientations described in the preceding section as starting points.

Fig. 6A shows the space explored by the adsorbed protein along the simulations expressed in terms of the angles α and φ for each of the nine binding minima found for Cyt^{2+}. In all cases we observe significant mobility with partially overlapping trajectories that correspond to the dynamic sampling of the SAM surface by the protein via the binding sites BD2 and BD3. Within the time scale of the simulations the amplitude of the motion is variable depending on the starting point, with α averaging 40° and φ ranging between 35° and 70°. However, the partial overlap of the different trajectories suggests even larger mobility at longer time scales. Also the BD1 site exhibits a large mobility but the exposed heme edge remains apart from the SAM surface over the entire simulation time and, thus, the site is not expected to be relevant for ET, as confirmed below.

The mobility of the adsorbed protein is expected to be affected by the charge density of the SAM. In order to asses the magnitude of this effect MD simulations were also performed for one selected

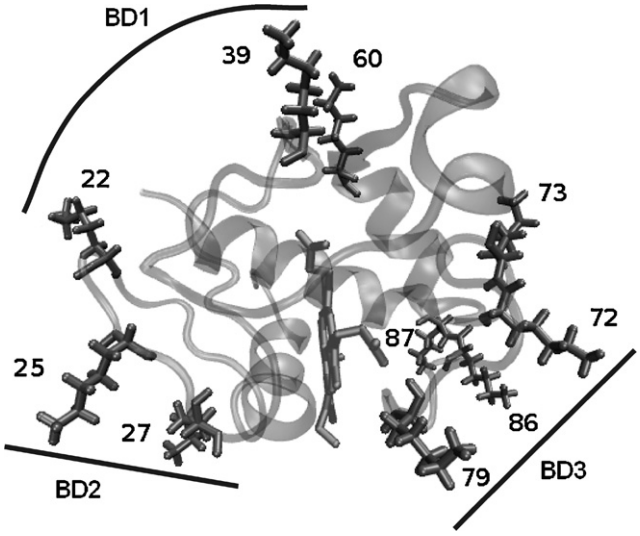

Fig. 5. Schematic representation of the three domains of Cyt for binding to a C_5-SAM with 10% ionization.

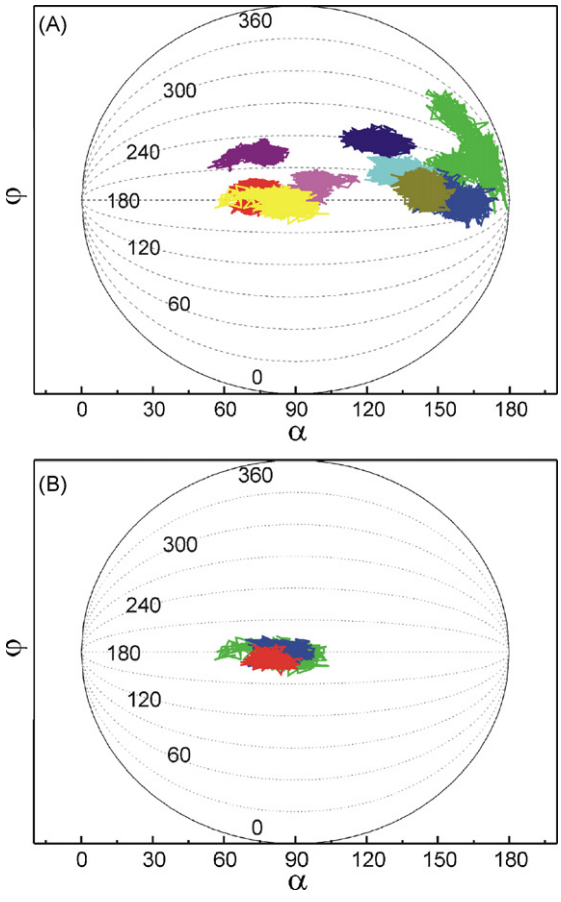

Fig. 6. (A) 5 ns MD simulation trajectories for Cyt^{2+} adsorbed to a C_5-SAM with 10% ionization. Each colour represents one of the nine binding minima used as starting points. Isolines indicate the φ values. (B) MD simulation trajectories for Cyt^{2+} adsorbed to a C_5-SAM with 10% (green), 25% (blue) and 50% (red) ionization using the minimum with $\alpha = 70^\circ$ and $\varphi = 172^\circ$ as starting point. (For interpretation of the references to colour in this figure legend, the reader is referred to the web version of the article.)

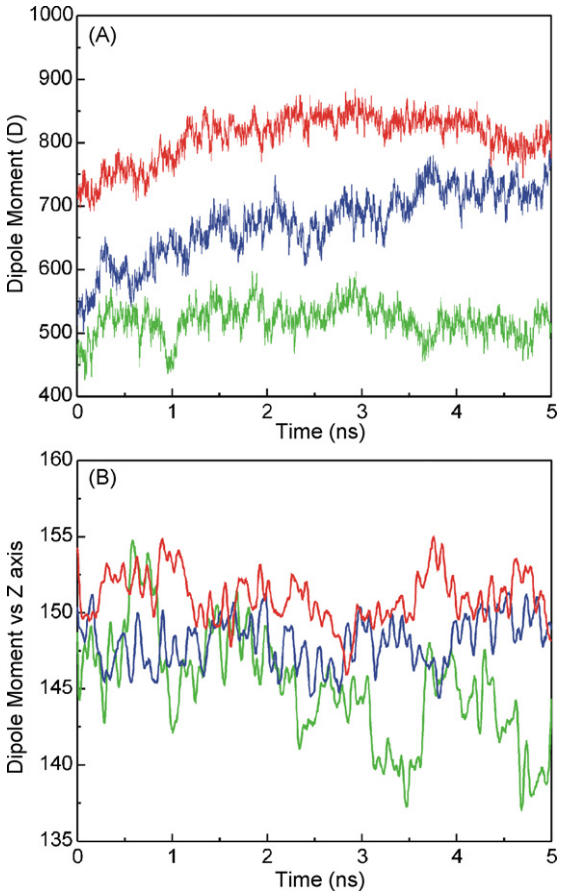

Fig. 7. Effect of the SAM ionization on (A) the dipole moment of Cyt^{2+} and (B) the angle between the dipole moment and the *Z*-axis. Green: 10% ionization. Blue: 25% ionization. Red: 50% ionization. (For interpretation of the references to colour in this figure legend, the reader is referred to the web version of the article.)

binding minimum at three different SAM ionization degrees of 10%, 25% and 50%. The results are shown in Fig. 6B. Taking the SAM with 10% ionization as a reference, the mobility of Cyt^{2+} in the α direction decreases by 38% and 44% for 25% and 50% ionization, respectively. The effect is also significant in the φ direction for which the mobility decreases by 13% and 22% for similar increments of the ionization degrees of the SAM.

Also the dipole moment of the protein is affected by the charge density of the SAM. As shown in Fig. 7A, the dipole moment increases with simulation time and is larger for the more ionized SAMs. These results are in very good agreement with previous calculations [35]. The increase of the dipole moment is mainly related to the rearrangement of amino acid side chains of Cyt in the electrostatic complexes and, therefore, do not have a direct correlation with the protein orientation defined in terms of the heme group. Indeed, the variability of the dipole angle *vs*. the *Z*-axis decreases with the ionization of the SAM (Fig. 7B).

The simulations do not consider the electric field that originates in the potential drop across the electrode/SAM/protein interface. Under these conditions the mobility of the protein is expected to be further reduced as a consequence of the alignment of the increased dipole moment with the electric field.

3.4. Fluctuations of the electronic coupling

The possible influence of the protein dynamics on the heterogeneous ET reaction was analyzed by determining the optimal electron pathways and the corresponding electronic coupling

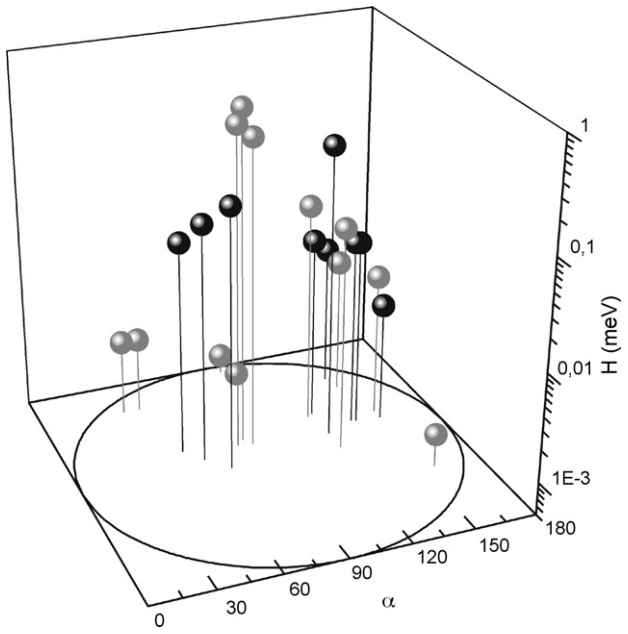

Fig. 8. Average electronic couplings obtained from the 5 ns simulations for selected minima represented in Fig. 4. Black circles: Cyt^{2+}. Grey circles: Cyt^{3+}.

parameters (H) along the 5 ns MD simulations for each of the Cyt/SAM complexes described above, with 10% ionization of the SAM. Pathways calculations were performed for 14 snapshots of each trajectory, i.e. each 0.4 ns. As expected, we observe large differences of H for starting orientations that differ significantly in terms of α and φ. The low affinity site BD1 corresponds to the smallest couplings with H values in the order of 10^{-4} meV and can be regarded as an electrochemically inactive orientation for practical purposes. In contrast, for the medium affinity site BD2 the average value of H is in the order of 0.1 meV and for the high affinity site BD3 it is ca. 0.01 meV (Fig. 8).

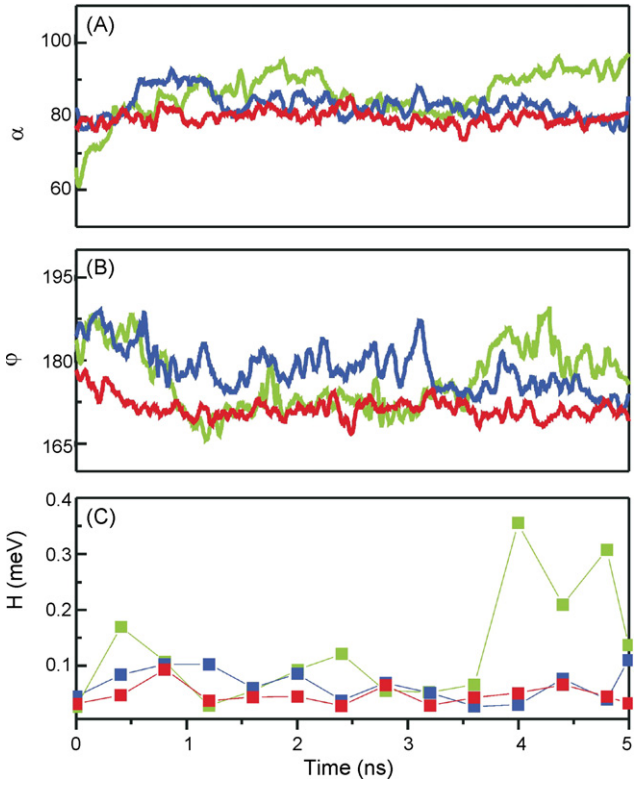

Fig. 9. MD simulations of Cyt^{2+} electrostatically adsorbed on C_5-SAM monolayers with different degrees of ionization. Green: 10% ionization. Blue: 25% ionization. Red: 50% ionization. (A)–(C) show the time evolution of the angles α and φ and of the electronic coupling, respectively. (For interpretation of the references to colour in this figure legend, the reader is referred to the web version of the article.)

Large fluctuations of H are also observed along the individual dynamics even for relatively small changes of angles. As an example, Fig. 9 shows the H values along the three trajectories from Fig. 6B. For the SAMs with 25% and 50% ionization H oscillates between 0.025 and 0.1 meV along the 5 ns simulation, although in general H is somehow smaller and less variable for 50% ionization. In contrast, for a 10%-deprotonated SAM the significantly larger mobility of Cyt allows for the exploration of the surface in search for better electron pathways, which results in oscillations of H from ca. 0.025–0.36 meV. Note that such a variation represents an acceleration of the electron transfer rate by a factor of ca. 200 as $k^{ET} \propto H^2$ [36], and may arise from relatively low amplitude motions of the protein with $\Delta\alpha \sim 5^\circ$ and $\Delta\varphi \sim 10^\circ$.

4. Conclusions

MD simulations show that adsorption of Cyt on electrodes coated with a SAM of 6-mercaptohexanoic acid leads to a broad distribution of orientations which differ in terms of electronic coupling by up to four orders of magnitude and, therefore, to a distribution of electron transfer rate constants that spans eight decades. The highest electronic couplings, in the range of 1 meV, are found for the binding domain of medium affinity (BD2) which involves lysines 25 and 27 as key amino acid residues. The electrostatic complex Cyt/SAM formed through the BD2 domain is not rigid and instead presents significant protein mobility, which for a 5 ns MD simulation is associated with variations of the electronic coupling by a factor of ca. 14, corresponding to a factor 200 for the electron tunnelling rate. The mobility of the protein is reduced upon increasing the degree of ionization of the SAM. As a consequence, the largest electronic couplings that can be achieved within the simulation time for a 50% ionized SAM are ca. four times lower than for 10% ionization.

These results suggest that experimentally determined ET rates represent a convolution of the dynamics of the electrostatic ensemble and the electronic couplings that characterize each of the individual protein orientations. Simulations predict a slow down of the measured rates upon rising the pH as a consequence of the reduced protein mobility that impairs establishing optimal electron pathways. This prediction agrees well with the experimental observations. TR-SERR measurements performed with Soret- and Q-band excitation yield essentially the same apparent rate constants for heterogeneous ET and protein reorientation, respectively. Furthermore, both apparent rate constants decrease to the same extent upon raising the pH. Thus, experiments indicate that protein reorientation is rate limiting.

It is important to note that simulated protein dynamics and experimentally determined reorientation occur in different time scales. Simulations, however, are not aimed to exactly reproduce the experiments, which occur in time scales not affordable by current computational power, but to yield an atomistic picture of how crucial protein dynamics can be in determining the efficiency of the interfacial ET reaction.

An essential difference between simulations and experiments is that in the second case protein reorientation occurs under the influence of the large electric field that results from the drop of the poised potential across the interface. Qualitatively, the effect of the interfacial electric field can be seen equivalent to an increase of the ionization degree of the SAM which, according to the simulations, results in reduced protein mobility and less efficient electron

pathways. Quantitatively, the effect can be significant. For example, ET rates of Cyt immobilized on Ag electrodes coated with thin SAMs, i.e. in the distance-independent regime, are nearly one order of magnitude slower than on Au electrodes. The difference has been attributed to the lower potential of zero charge for Ag that leads to larger electric fields [21]. Recently it has been found that the rate of reorientation of yeast Cyt adsorbed on SAM-coated electrodes is slower than for horse heart Cyt under otherwise identical conditions [37]. The finding was rationalized in terms of the larger dipole moment of the yeast protein that imposes a larger activation barrier for reorientation within the field. Furthermore, the average orientation of Cyt on SAM-coated electrodes has been found to be potential-dependent and the rate of reorientation is more than two orders of magnitude faster at thicker spacers, i.e. at lower electric fields [23]. Thus, reorientation of the adsorbed protein that in the absence of external electric fields is predicted to occur in the ns range by the MD simulations is likely to be slowed down to the ms range in actual electrodes under the influence of electric fields of ca. 109 V m^{-1} [34], as observed experimentally.

In summary, TR-SERR experiments and simulations reported here provide a consistent picture of the heterogeneous ET dynamics of Cyt at SAM-coated electrodes. The observed ET rate should be interpreted as an average value of a dynamic ensemble, and it is the result of the interplay of reorientation rates and tunnelling probabilities. For long tethers and low charge densities of the SAMs interfacial electric fields are low and, therefore, reorientation dynamics is sufficiently fast compared to electron tunnelling, leading to a "normal" distance dependence of the ET rates. For short tethers charge densities of the SAMs are larger as the pK_a values decrease with distance and, at the same time, local electric fields increase. Under these conditions protein mobility is significantly restricted and thus becomes the rate limiting event.

This conclusion, which refers to Cyt electrostatically adsorbed on metal electrodes coated with SAMs of ω-carboxylalkanethiols, may also be valid for other cases of immobilized redox proteins that have been reported to show unusual distance dependencies of the ET rates [10,12,14,15].

Note that Cyt exerts its natural electron carrier function at a membrane interface where the local pH is constantly changing as a result of the proton pumping activity of the respiratory complexes and the proton consumption by ATP-synthase. Thus, it is very likely that the variable electric field generated by the proton gradient across the membrane, as well as changes of the local pH, influence the dynamics of Cyt ET reaction *in vivo*, as suggested by the present studies with a simplified model system.

The combined experimental–computational approach reported here allows for understanding in depth the results from bioelectrochemical experiments, thus opening new perspectives for basic and applied studies that involve redox proteins at electrodes with biomimetic or sensing purposes.

Acknowledgments

Financial support by ANPCyT (PICT 2006-459 and 2007-1650) and UBA (08-X625) is gratefully acknowledged. Computer simulations were done using resources kindly provided by the Open Science Grid, which is supported by the National Science Foundation and the U.S. Department of Energy's Office of Science. DAP and DFM are CONICET fellows. MAM and DHM are members of CIC-CONICET. PH acknowledges the support by the DFG (Sfb498, Cluster of Excellence "UniCat").

References

[1] F.A. Armstrong, N.A. Belsey, J.A. Cracknell, G. Goldet, A. Parkin, E. Reisner, K.A. Vincent, A.F. Wait, Chem. Soc. Rev. 38 (2009) 36.
[2] A. Brajter-Toth, J.Q. Chambers (Eds.), Electroanalytical Methods for Biological Material, Marcel Dekker, Inc., New York, 2002.
[3] D.H. Murgida, P. Hildebrandt, Chem. Soc. Rev. 37 (2008) 937.
[4] E. Katz, I. Willner, Angew. Chem. Int. Ed. 43 (2004) 6042.
[5] J.A. Cracknell, K.A. Vincent, F.A. Armstrong, Chem. Rev. 108 (2008) 2439.
[6] J.J. Feng, P. Hildebrandt, D.H. Murgida, Langmuir 24 (2008) 1583.
[7] D.H. Murgida, P. Hildebrandt, Acc. Chem. Res. 37 (2004) 854.
[8] D.H. Murgida, P. Hildebrandt, Phys. Chem. Chem. Phys. 7 (2005) 3773.
[9] D.H. Murgida, P. Hildebrandt, J. Am. Chem. Soc. 123 (2001) 4062.
[10] T. Albrecht, Ph.D. thesis, Technische Universität Berlin, 2003.
[11] A. Avila, B.W. Gregory, K. Niki, T.M. Cotton, J. Phys. Chem. B 104 (2000) 2759.
[12] Q.J. Chi, J.D. Zhang, J.E.T. Andersen, J. Ulstrup, J. Phys. Chem. B 105 (2001) 4669.
[13] D.E. Khoshtariya, J.J. Wei, H.Y. Liu, H.J. Yue, D.H. Waldeck, J. Am. Chem. Soc. 125 (2003) 7704.
[14] K. Fujita, N. Nakamura, H. Ohno, B.S. Leigh, K. Niki, H.B. Gray, J.H. Richards, J. Am. Chem. Soc. 126 (2004) 13954.
[15] F.A. Armstrong, N.L. Barlow, P.L. Burn, K.R. Hoke, L.J.C. Jeuken, C. Shenton, G.R. Webster, Chem. Commun. (2004) 316.
[16] T.M. Nahir, E.F. Bowden, J. Electroanal. Chem. 410 (1996) 9.
[17] T.D. Dolidze, S. Rondinini, A. Verto-Va, D.H. Waldeck, D.E. Khoshtariya, Biopolymers 87 (2007) 68.
[18] D.H. Murgida, P. Hildebrandt, J. Wei, Y.F. He, H.Y. Liu, D.H. Waldeck, J. Phys. Chem. B 108 (2004) 2261.
[19] J.J. Wei, H.Y. Liu, A.R. Dick, H. Yamamoto, Y.F. He, D.H. Waldeck, J. Am. Chem. Soc. 124 (2002) 9591.
[20] J.J. Wei, H.Y. Liu, D.E. Khoshtariya, H. Yamamoto, A. Dick, D.H. Waldeck, Angew. Chem. Int. Ed. 41 (2002) 4700.
[21] H.J. Yue, D. Khoshtariya, D.H. Waldeck, J. Grochol, P. Hildebrandt, D.H. Murgida, J. Phys. Chem. B 110 (2006) 19906.
[22] D.H. Murgida, P. Hildebrandt, J. Phys. Chem. B 106 (2002) 12814.
[23] A. Kranich, H.K. Ly, P. Hildebrandt, D.H. Murgida, J. Am. Chem. Soc. 130 (2008) 9844.
[24] B. Rai, P. Sathish, C.P. Malhotra, Pradip, K.G. Ayappa, Langmuir 20 (2004) 3138.
[25] D.A. Case, T.E. Cheatham III, T. Darden, H. Gohlke, R. Luo, K.M. Merz Jr., A. Onufriev, C. Simmerling, B. Wang, R. Woods, J. Comput. Chem. 26 (2005) 1668.
[26] D.E. Bikiel, L. Boechi, L. Capece, A. Crespo, P.M. De Biase, S. Di Lella, M.C.G. Lebrero, M.A. Marti, A.D. Nadra, L.L. Perissinotti, D.A. Scherlis, D.A. Estrin, Phys. Chem. Chem. Phys. 8 (2006) 5611.
[27] S. Park, K. Schulten, J. Chem. Phys. 120 (2004) 5946.
[28] A. Onufriev, D. Bashford, D.A. Case, Proteins: Struct. Funct. Bioinform. 55 (2004) 383.
[29] H.J.C. Berendsen, J.P.M. Postma, W.F. Vangunsteren, A. Dinola, J.R. Haak, J. Chem. Phys. 81 (1984) 3684.
[30] W.H. Koppenol, J.D. Rush, J.D. Mills, E. Margoliash, Mol. Biol. Evol. 8 (1991) 545.
[31] D.N. Beratan, J.N. Onuchic, J.N. Betts, B.E. Bowler, H.B. Gray, J. Am. Chem. Soc. 112 (1990) 7915.
[32] D.N. Beratan, J.N. Onuchic, J.R. Winkler, H.B. Gray, Science 258 (1992) 1740.
[33] I.D.G. Macdonald, W.E. Smith, Langmuir 12 (1996) 706.
[34] D.H. Murgida, P. Hildebrandt, J. Phys. Chem. B 105 (2001) 1578.
[35] J. Zhou, J. Zheng, S.Y. Jiang, J. Phys. Chem. B 108 (2004) 17418.
[36] A.M. Kuznetsov, J. Ulstrup, Electron Transfer in Chemistry and Biology. An Introduction to the Theory, 1 ed., Wiley, Chichester, 1991.
[37] J.J. Feng, U. Kuhlmann, D.H. Murgida, T. Utesch, M. Mroginski, P. Hildebrandt, I. Weidinger, J. Phys. Chem. B 112 (2008) 15202.